Local spectral model of geoid and geoid-to-quasigeoid separation in North America

Ismael Foroughi*, Robert Kingdon, Michael Sheng, and Marcelo Santos
Department of Geodesy and Geomatics, University of New Brunswick, Fredericton, Canada.

1 Introduction

Knowledge of the external gravitational field of the Earth has been significantly improved by the gravity-dedicated satellite missions, especially at long-to-medium wavelengths. The medium-to-short wavelengths of the gravitational field, however, are usually provided by terrestrial gravity observations and topographic data. The long-wavelength gravitational spectrum comprises mainly the signature of deep mantle density heterogeneities, while the medium-to-short wavelengths are dominated by the signal from more shallow sources within the lithosphere including the shape of terrain (on land) and the ocean-floor relief (offshore).

The external gravitational field of the Earth can directly be used to model the geoid and related gravitational field quantities over the world's oceans and smaller seas. Over continents, geoid determination using an external gravitational field model requires modeling topographical effects. In global studies these are often ignored, assuming that the gravitational contribution of topography affects mainly the short-wavelength (higher-degree) spectrum of the gravitational field while the long-wavelength effect is small or completely negligible. In local studies, the topographic correction needs to be accounted for. The usual way of applying topographic correction to gravimetric geoid models computed in spectral way is by applying a Bouguer correction (e.g. Barthelmes 2009). In this study, we propose a spectral topographic model as a substitute to the Bouguer correction to compute geoid models in land areas, and we demonstrate that a rigorous topographic correction can differ significantly from the Bouguer correction especially in areas with complex topography. To investigate these differences, we present the numerical method of computing the gravitational field quantities on the geoid from the external gravitational field model. This method utilizes expressions derived in the spectral domain for the gravimetric forward modelling of topographic masses, and for the indirect gravimetric modelling of masses distributed inside the geoid.

The methodology and data acquisition are summarized in section 2. The results are presented and discussed in sections 3.

2 Methodology and data acquisition

Using the spectral expressions; the disturbing potential (T) of the Earth can only be computed at the topographic surface, but for computing this value at the geoid the disturbing potential must be harmonically downward continued. In order to provide a space where the potential is harmonic, we propose decomposing the Erath's gravitational field into topographic and non-topographic parts. The topographic part (V^T) represents the gravitational contribution of topographic masses, while the non-topographic (T^{NT}) part accounts for the gravitational contribution of masses distributed inside the geoid. Atmospheric masses are neglected, in this development, but could be accounted for with minor modifications.

By this analogy, the disturbing potential at the topographic surface is computed as:

$$T(r_t, \Omega) = T^{NT}(r_t, \Omega) + V^T(r_t, \Omega). \quad (1)$$

By arbitrarily adding and subtracting $T^{NT}(r_t, \Omega)$ to the corresponding equation for disturbing potential at geoid we get:

$$T(r_g, \Omega) = T^{NT}(r_g, \Omega) + [T^{NT}(r_t, \Omega) - T^{NT}(r_t, \Omega)] + V^T(r_g, \Omega), \quad (2)$$

and by substituting $T^{NT}(r_t, \Omega)$ from Eq. (1) to Eq. (2) we get:

$$T(r_g,\Omega) = T(r_t,\Omega) + \left[T^{NT}(r_g,\Omega) - T^{NT}(r_t,\Omega)\right] + \left[V^T(r_g,\Omega) - V^T(r_t,\Omega)\right], \quad (3)$$

where, r_g and r_t are the geocentric radii of the points at the geoid and topographic surfaces respectively, and $\Omega = (\phi, \lambda)$ is the spherical direction with the spherical latitude ϕ and longitude λ.

Eq. (3) relates the disturbing potential values on the geoid and at the topographic surface by means of the topographic potential difference $V^T(r_g,\Omega) - V^T(r_t,\Omega)$ and the no-topography disturbing potential difference $T^{NT}(r_g,\Omega) - T^{NT}(r_t,\Omega)$. Following the procedure proposed in Santos et al. (2006), we further treat the topographic potential individually for the gravitational contributions of the (constant) reference and (spatially-variable) anomalous topographic density distributions:

$$T(r_g,\Omega) = T(r_t,\Omega) + \left[T^{NT}(r_g,\Omega) - T^{NT}(r_t,\Omega)\right] + \left[V^{T,\rho^T}(r_g,\Omega) - V^{T,\rho^T}(r_t,\Omega)\right] + \left[V^{T,\delta\rho^T}(r_g,\Omega) - V^{T,\delta\rho^T}(r_t,\Omega)\right] \quad (4)$$

where V^{T,ρ^T} and $V^{T,\delta\rho^T}$ are the topographic potentials of the reference and anomalous topographic density, respectively.

The disturbing potential at the topographic surface in Eq. (4) is computed in the spectral domain. The topographic density contribution (i.e., the topographic potential difference) in Eq. (4) comprises the contributions of the masses of reference density and those of anomalous topographic density. The topographic density contribution is evaluated from available digital terrain and density models using gravimetric forward modelling. The computation of the non-topographic contribution (i.e., the no-topography disturbing potential difference) in Eq. (4) requires an additional numerical step of subtracting the topographic potential from the disturbing potential at the topographic surface. Taking into consideration the decomposition of the topographic potential into the reference and anomalous density contributions in Eq. (1), this numerical step is defined as

$$T^{NT}(r_t,\Omega) = T(r_t,\Omega) - V^{T,\rho^T}(r_t,\Omega) - V^{T,\delta\rho^T}(r_t,\Omega). \quad (5)$$

The spectral expressions for computing the topographic and non-topographic components are summarized in Tenzer et al. (2015).

We applied methods for spherical harmonic analysis and synthesis of global terrain data to compute the topographic potential based on the reference density of $2670\ kg\ m^{-3}$. The influence on topographic potential of the anomalous density distribution was evaluated individually for the contributions of large lakes, polar ice sheets, sediments, and bedrock density variations. These contributions were computed in terms of their density anomaly taken relative to the reference topographic density. The global models used for computations comprised the Earth2014 (degree/order 2160) (Hirt and Rexer 2015) datasets of terrain, ice thickness and inland bathymetry and the CRUST1.0 (Laske et al. 2013) sediment and consolidated crustal data. The freshwater density of 1000 $kg\ m^{-3}$ and the density of glacial ice of 917 $kg\ m^{-3}$ were adopted for computing the gravitational potentials of lakes and ice respectively. The sediment and consolidated crustal density data retrieved from the CRUST1.0 global crustal seismic model was used to compute the contributions of sediments and bedrock. The gravitational contribution of masses distributed inside the geoid was computed in terms of the no-topographic disturbing potential difference. This computation was realized as follows: the EIGEN-6C4 coefficients (Förste et al., 2014). The computation area were chosen in the North-American continent and on 5x5 arc-min spherical grid points.

The differences between disturbing potential computed at the surface of the Earth and evaluated at the geoid further were used to analyze the harmonic coefficients of the geoid-to-quasigeoid separation.

3 Numerical results and conclusion

The differences between disturbing potential of topographic and non-topographic mass components computed at topographic surface and geoid are shown in Figure 1, and statistics of these plots are summarized in Table 1.

Figure 1: Differences between $T(r_t, \Omega)$ and $T(r_g, \Omega)$in terms of mass components, $[\boldsymbol{m^2/s^2}]$

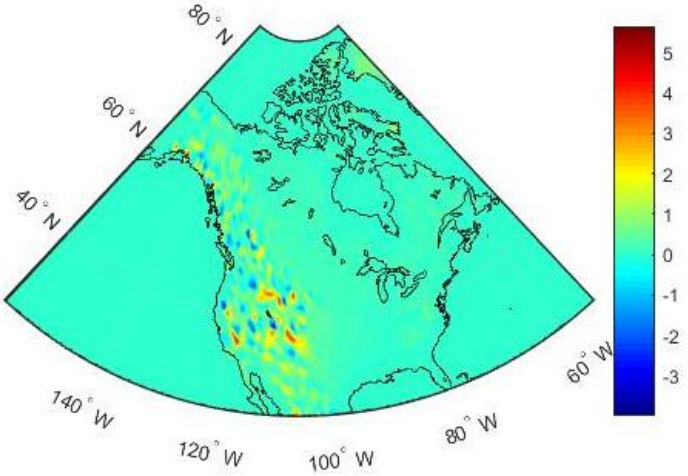

Topographic of mean density $\boldsymbol{\delta T^{\rho^T}}$

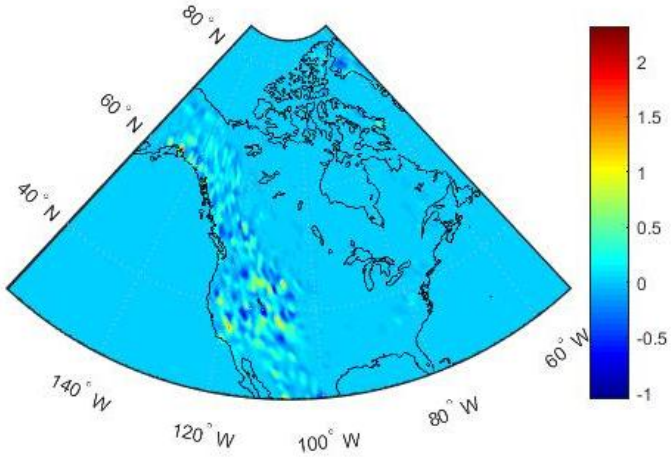

Ice thickness $\boldsymbol{\delta T^{\rho^{Ice}}}$

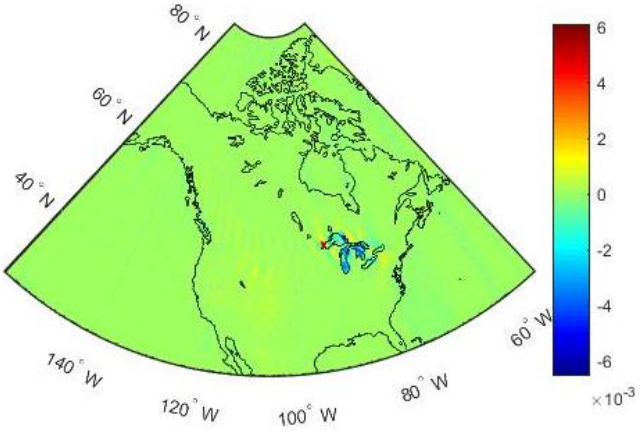

Inland bathymetric $\boldsymbol{\delta T^{\rho^{lake}}}$

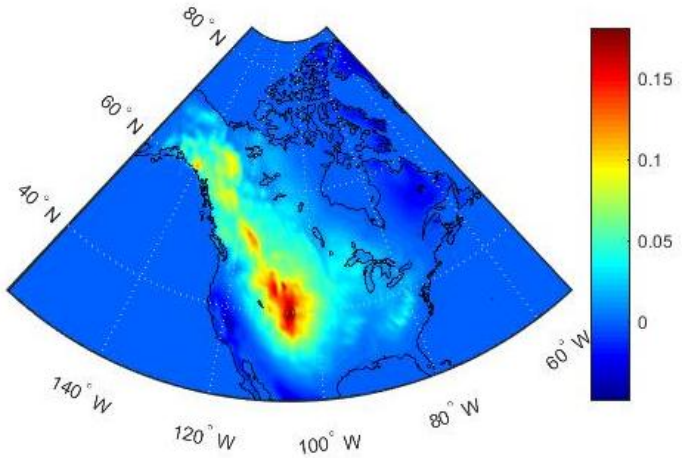

Sediment $\boldsymbol{\delta T^{\rho^{Sediment}}}$

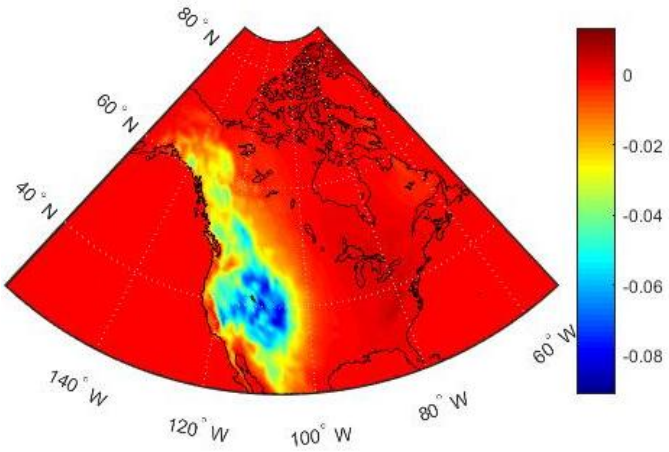

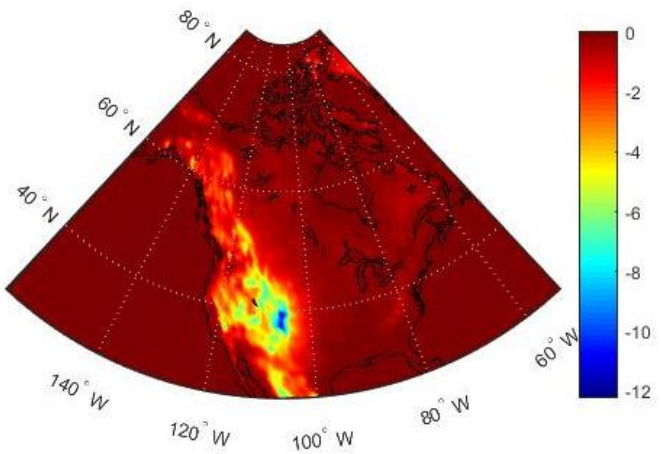

Bedrock $\delta T^{\rho^{Bedrock}}$ No-Topography δT^{NT}

	MIN $[m^2/s^2]$	MAX $[m^2/s^2]$	MEAN $[m^2/s^2]$	STD $[m^2/s^2]$
δT^{ρ^T}	-4.28	5.75	0.08	0.38
$\delta T^{\rho^{Ice}}$	-1.12	2.36	0.01	0.110
$\delta T^{\rho^{lake}}$	-0.007	0.007	0.0	0.0
$\delta T^{\rho^{Sediment}}$	-0.05	0.18	0.01	0.02
$\delta T^{\rho^{Bedrock}}$	-0.09	0.01	0.0	0.01
δT^{NT}	-12.67	0.05	-0.37	0.96

The numerical results revealed that the differences between the disturbing potential values computed on the geoid and at the topographic surface are significant, particularly in the mountainous regions with complex geology and over polar areas with the largest continental glacial cover. According to our estimates these differences globally vary from -41.8 to 2.7 m^2/s^2. The largest contribution to these potential differences is attributed to the gravitational contribution of mass density heterogeneities inside the geoid. The topographic potential differences are typically one order of the magnitude smaller (in absolute sense) than the non-topographic contribution. The contributions of sediments and bedrock are less pronounced, with the estimated variations less than ± 1.0 m^2/s^2. The contribution of lakes reaches the maximum over the Great Lakes.

The differences between normal and rigorous orthometric height has never been computed for the North-American continent in rigorous spectral way. Due to time-consuming numerical integrations of computing rigorous orthometric height spatially, the proposed model of this study can be used as accurate-enough substitute. The roughness of topography is treated rigorously here which in other studies is approximated.

4 References

Barthelmes, F. (2009). "Definition of functionals of the geopotential and their calculation from spherical harmonic models." Scientific Technical Report STR09/02. Potsdam.

Förste C, Bruinsma SL, Abrikosov O, Lemoine J-M, Schaller T, Götze H-J, Ebbing J, Marty J-C, Flechtner F, Balmino G, Biancale R (2014) EIGEN-6C4 The latest combined global gravity field model including GOCE data up to degree and order 2190 of GFZ Potsdam and GRGS Toulouse; presented at the 5th GOCE User Workshop, Paris, 25-28 November 2014

Hirt C, Rexer M (2015) Earth2014: 1 arc-min shape, topography, bedrock and ice-sheet models - available as gridded data and degree-10,800 spherical harmonics, Int J App Earth Obs Geoinf 39: 103-112

Laske G, Masters G, Ma Z, Pasyanos M (2013) Update on CRUST1.0 - A 1-degree Global Model of Earth's Crust, Geophys Res Abst, 15, Abstract EGU2013-2658

Santos, M., Vaníček, P., Featherstone, W., Kingdon, R., Ellmann, A., Martin, B.-A., Tenzer, R. (2006). The relation between rigorous and helmert's definition of orthometric heights. Journal of Geodesy, 80(12), 691–704.

Tenzer R, Hirt Ch, Claessens S, Novák P (2015a) Spatial and spectral representations of the geoid-to-quasigeoid correction. Surv Geophys 36(5): 627-658